Supplementary Information for

"Selection of Landing Sites for the Chang'E-7 Mission Using Multi-Source Remote Sensing Data"

Fei Zhao, Pingping Lu, Tingyu Meng, Yanan Dang, Yao Gao, Zihan Xu, Robert Wang and Yirong Wu

Contents of this file:

Supplementary Figures S1-7

Supplementary Tables S1-4

1. Supplementary Figure

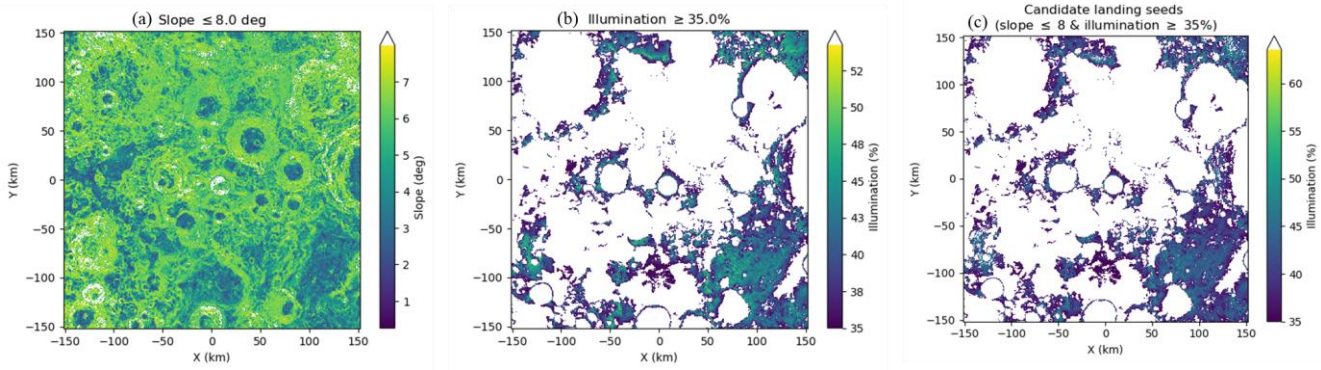


Figure S1. Factors influencing landing site selection. (a) Slope ≤ 8°; (b) Average illumination ≥ 35%; (c) Seeds of landing region that satisfy both the slope and illumination requirements. X and Y are the Cartesian coordinates in the south polar stereographic projection.

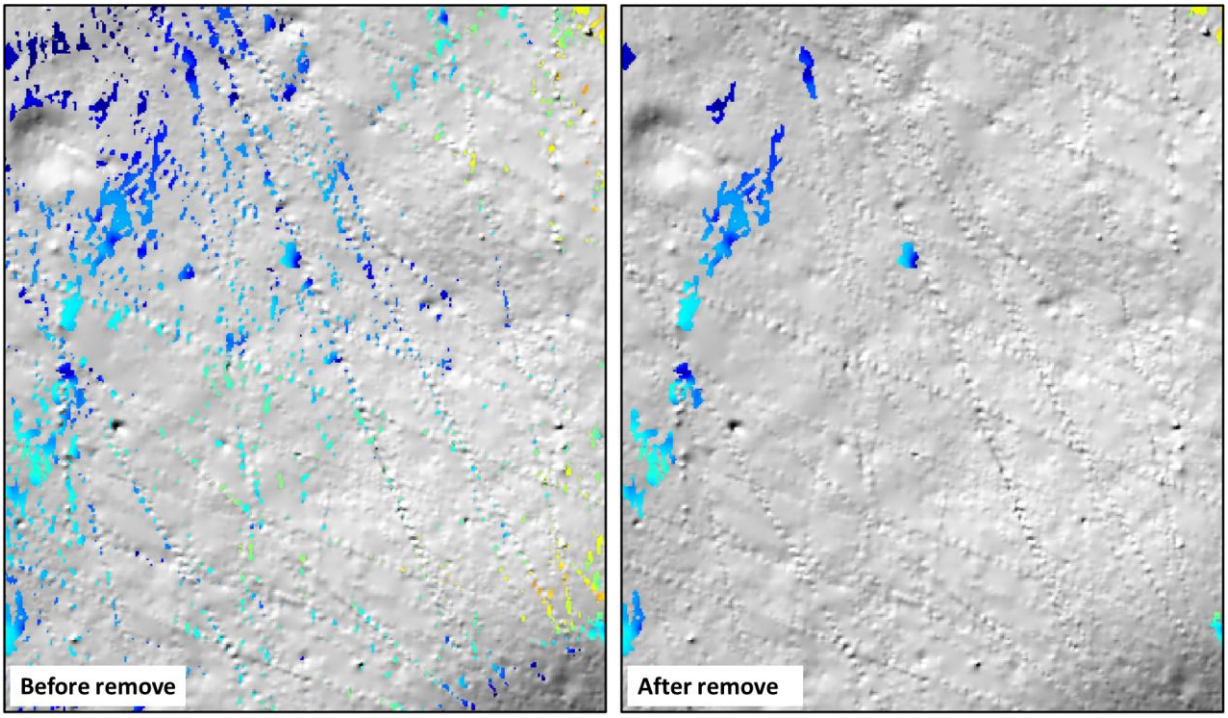


Figure S2. Removal of artifact seeds in the seed map (colored pixels) of landing cells, caused by inconsistencies in the LOLA topography data (see the artifact streaks in the background gray hillshade image).

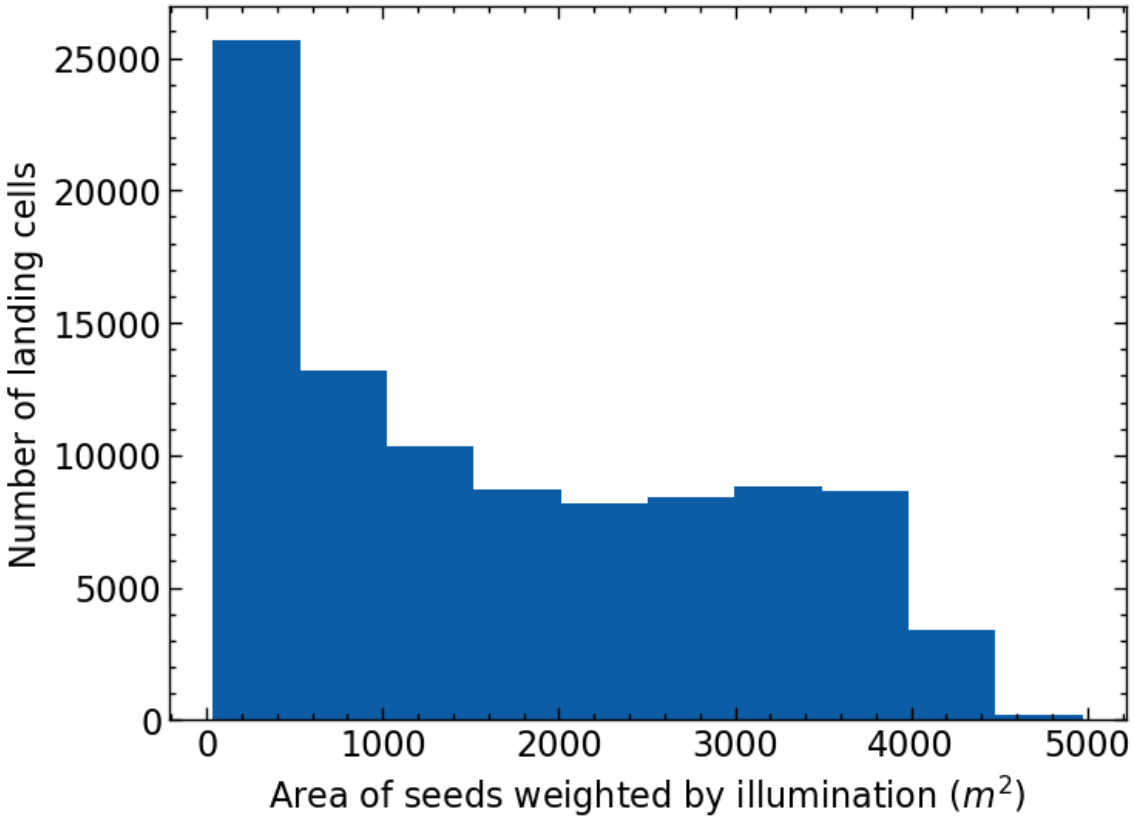


Figure S3. Statistical distribution of the areas of seeds within candidate landing cells, weighted by illumination.

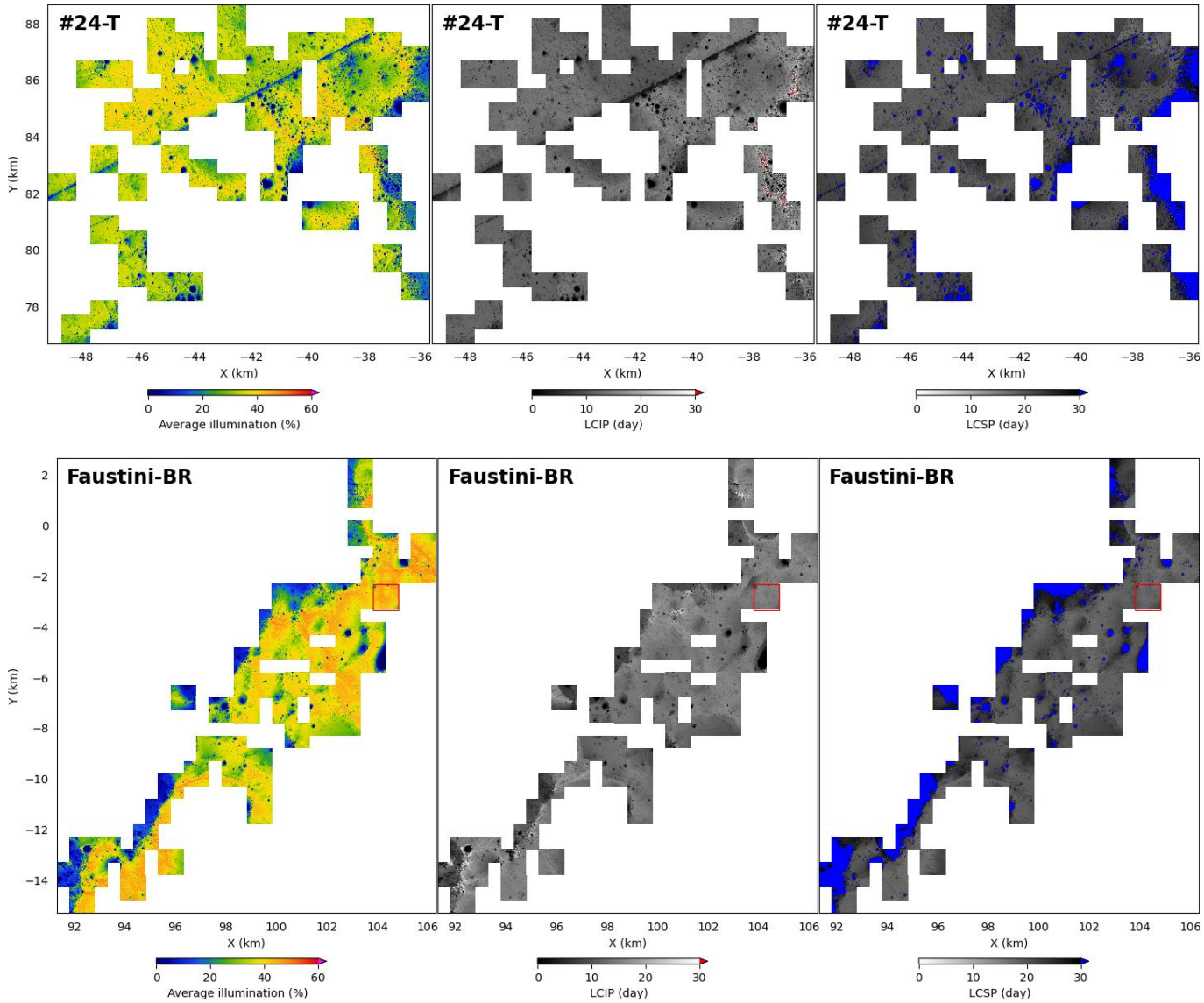


Figure S4. High-resolution illumination characteristics for six of the eight optimal landing regions: #24-T, Faustini-BR, de Gerlache-B, de Gerlache-TR, #12-TR, and de Gerlache-TL. For the remaining two optimal landing regions, de Gerlache-BL and Shackleton-L, refer to the main text. The average illumination represents the mean visible fraction of the solar disk from October 1, 2026, to October 1, 2034. LCIP and LCSP indicate the longest continuous illuminated and shadowed periods, respectively, during the time frame from October 1, 2026, to October 1, 2027. The optimal landing site (cell) with the highest average illumination within each landing region is highlighted with a red box (1 km × 1 km). The DEMs used for simulating the illumination conditions have a resolution of 10 m/pixel for #24-T and Faustini-BR, while the resolution is 5 m/pixel for the other regions.

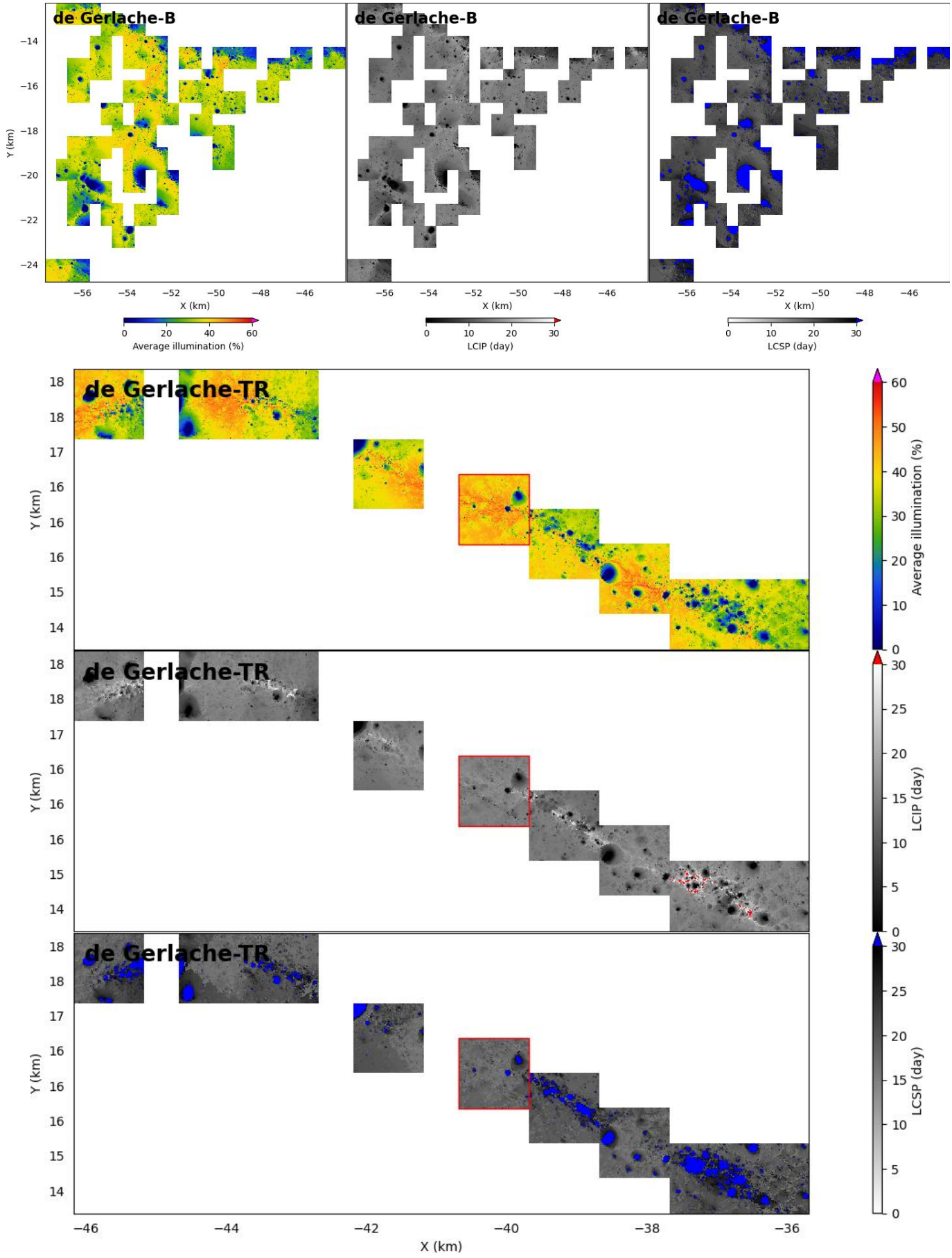


Figure S4. Continued.

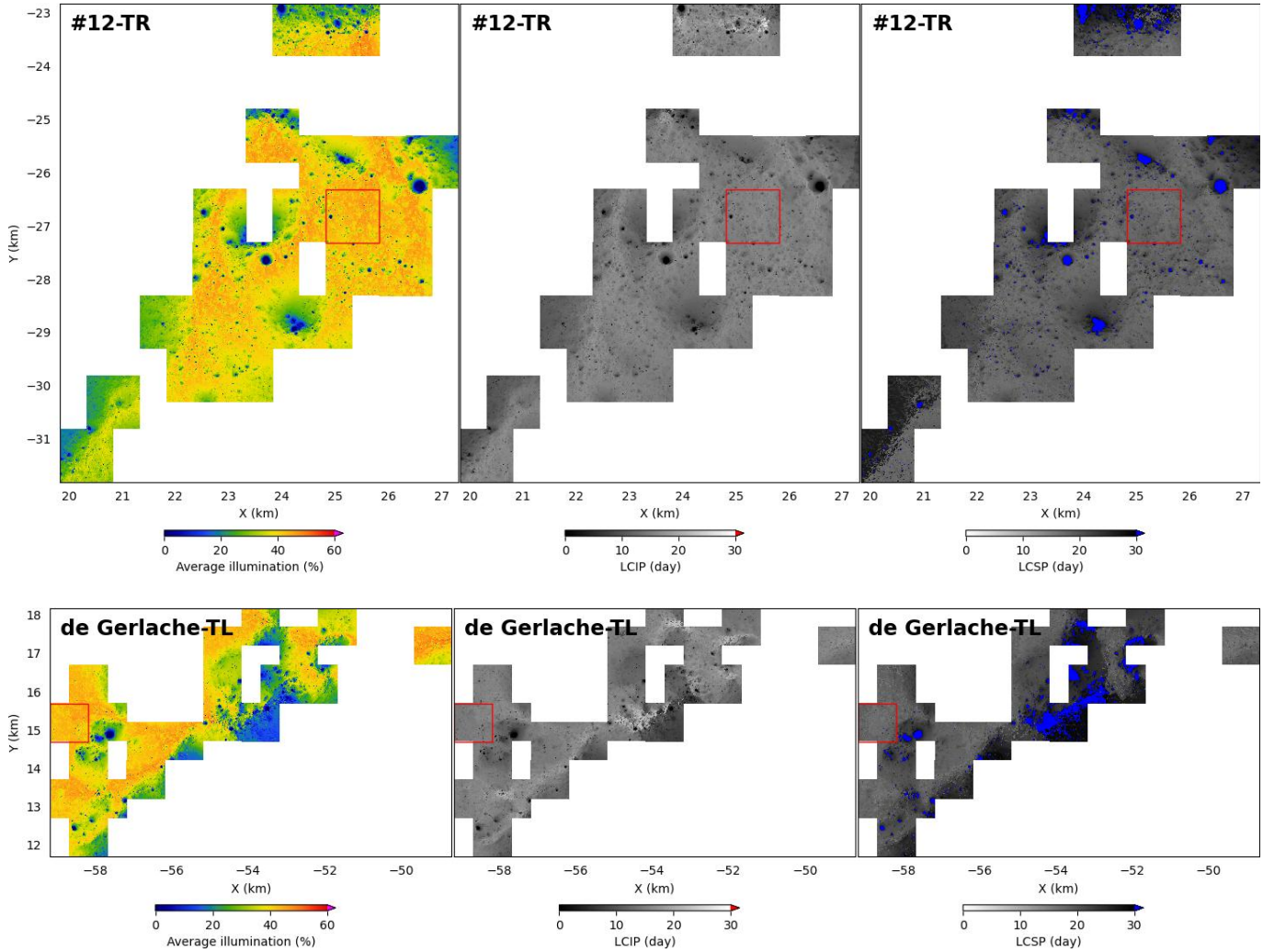


Figure S4. Continued.

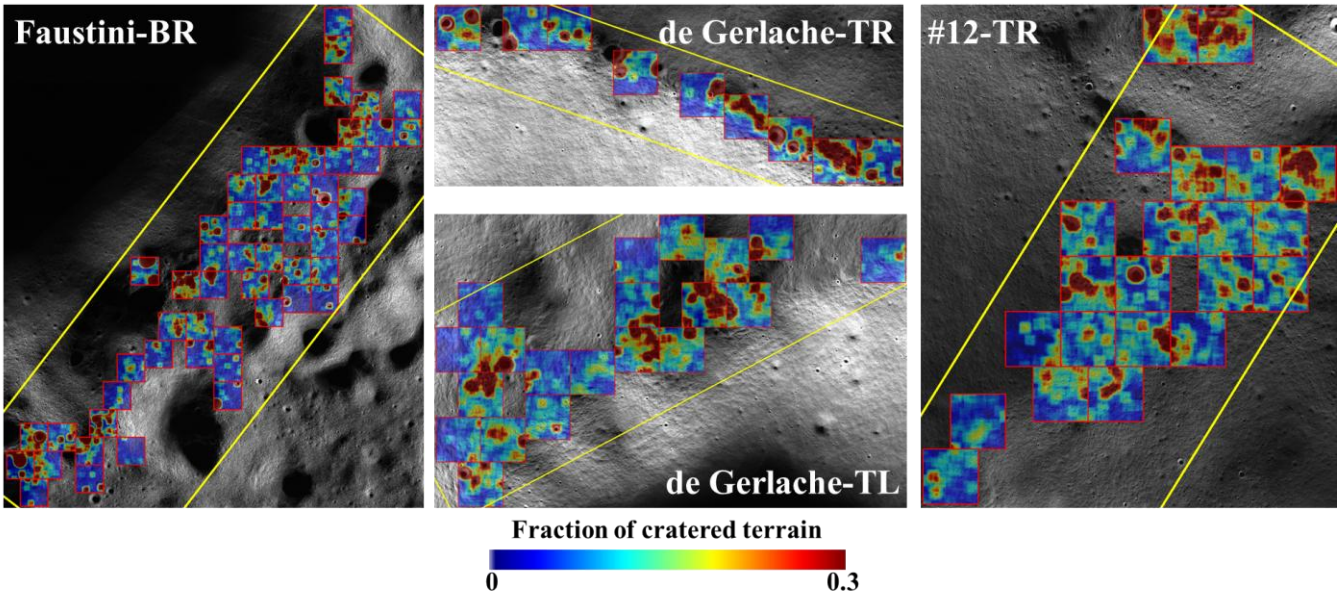


Figure S5. Distribution of the area fraction of cratered terrain within a 100 m radius window overlaid on the 1m/pixel NAC images for the selected landing regions: Faustini-BR, de Gerlache-TR, de Gerlache-TL, and #12-TR. The yellow box indicates the boundary of the landing region, while the red boxes represent 1 km × 1 km landing cells. The other two landing regions, de Gerlache-BL and Shackleton-L, are described in the main text.

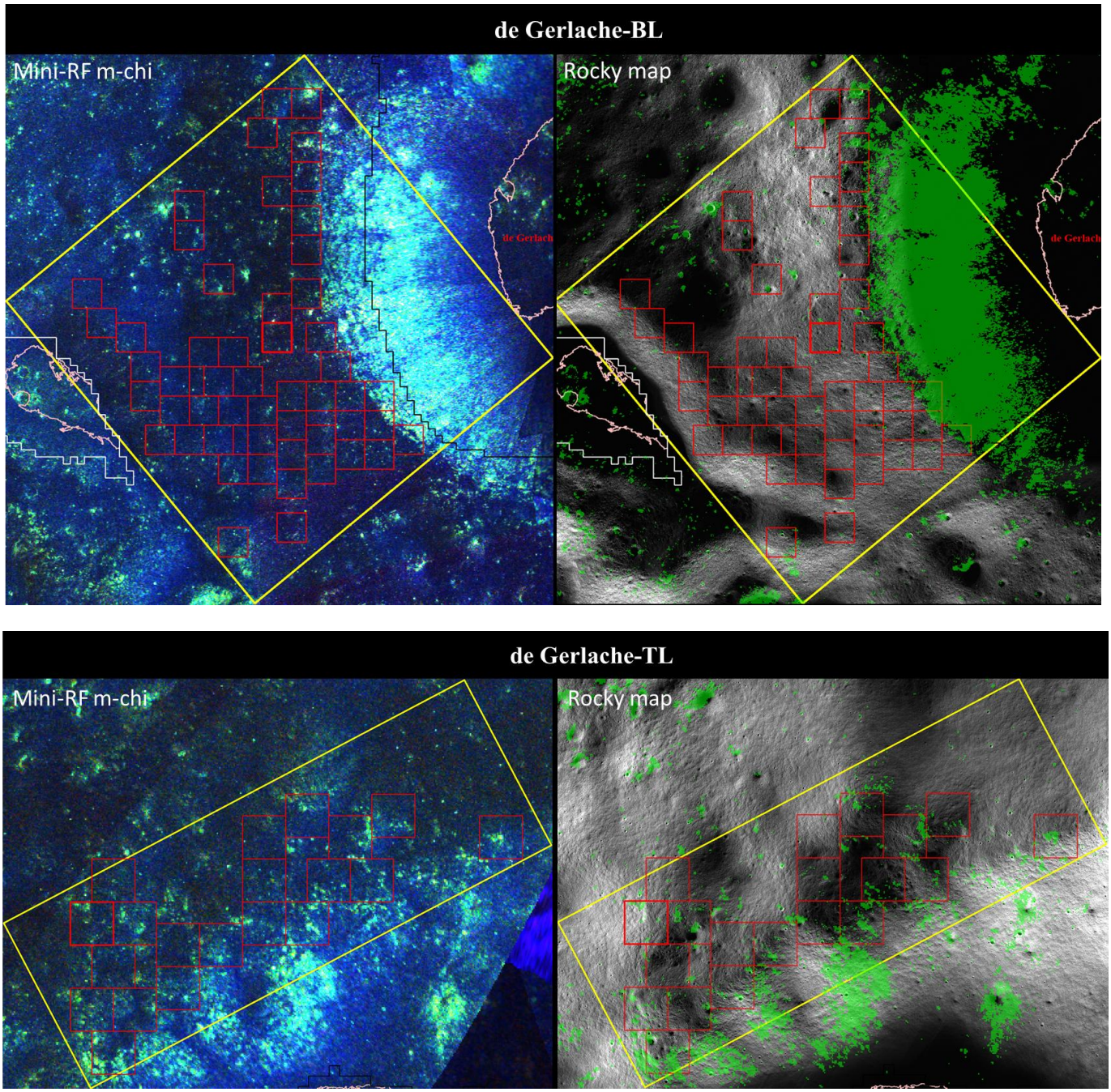


Figure S6. Distribution of rocky areas in the selected landing regions: de Gerlache-BL, de Gerlache-TL, #12-TR, de Gerlache-TR, and Shackleton-L. (Left column) Mini-RF m-chi decomposition images; (Right column) Distribution of rocky areas (green patches) overlaid on 1 m/pixel NAC images. Note that Mini-RF radar images do not cover de Gerlache-TR and Shackleton-L, so the rocky areas are manually identified from the NAC images. The yellow box indicates the boundary of the landing region, while the red boxes represent 1 km × 1 km landing cells. The Faustini-BR landing region is described in the main text.

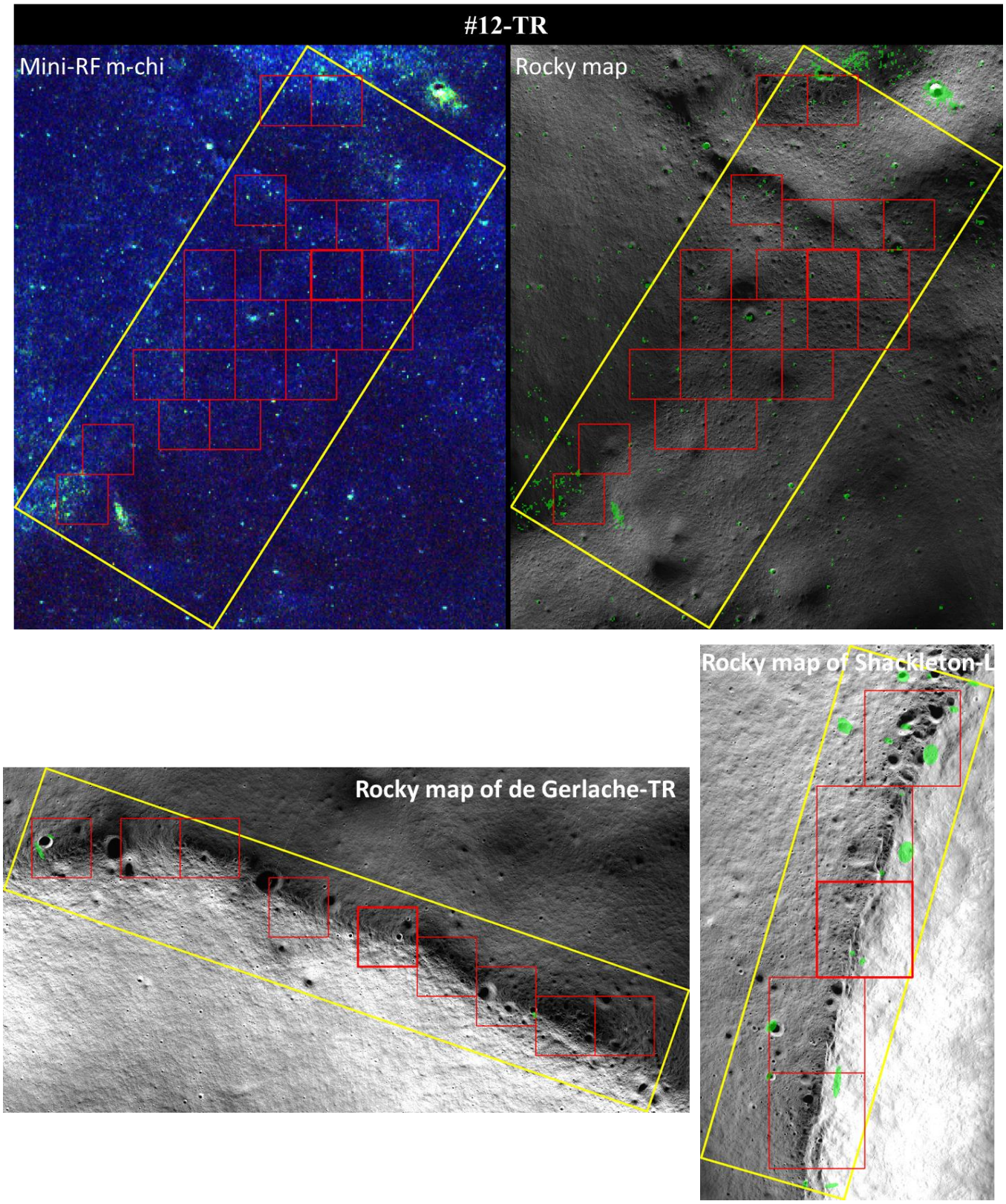


Figure S6. Continued.

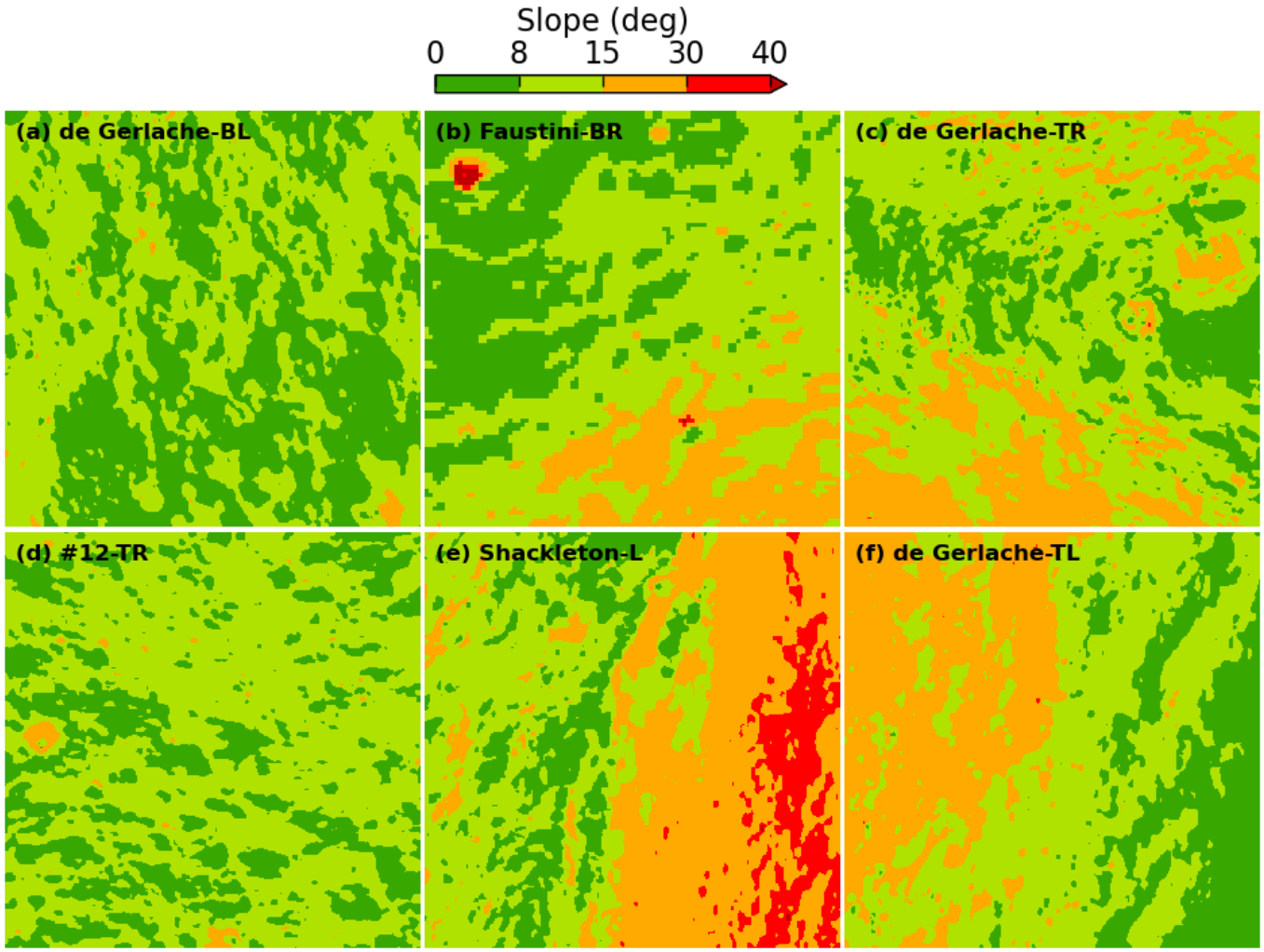


Figure S7. Distribution of slopes within the selected landing sites: (a) de Gerlache-BL; (b) Faustini-BR; (c) de Gerlache-TR; (d) #12-TR; (e) Shackleton-L; (f) de Gerlache-TL. The slopes are derived from the 5 m/pixel DEM, with an effective baseline of 10 m.

2. Supplementary Table

Table S1. Summary of the remote sensing data used in this study.

Data	Resolution	Purpose	Source
Mean sublimation rate, mean temperature	240 m/pixel	To define the cold traps	11 years of Diviner surface temperature measurements, [69]
LRO averaged LEND CSETN counts data	Binned into 0.5° × 0.5°	Quantify the hydrogen abundance	https://ode.rsl.wustl.edu/moon/productsearch, [76]
M3 water ice detections	Point size: 240 m × 240 m	Evaluate the likelihood of water ice presence in cold traps	https://trek.nasa.gov/moon/TrekWS/rest/cat/data/stream?label=SP_IceLoc_280m, [9]
South pole 5 m DEM	5 m/pixel	Slope and illumination calculation	https://pgda.gsfc.nasa.gov/products/81, [82]
LOLA DEM	10, 20, 40, 60, 120 m/pixel	Slope and illumination calculation, hillshade generation	LOLA PDS Data Node: https://imbrium.mit.edu/ [60]
South pole average illumination map	60 m/pixel	Preliminary screening of landing sites	LOLA PDS Data Node: https://imbrium.mit.edu/, [60]
South pole permanently shadowed regions (PSRs)	N/A	Evaluate the likelihood of water ice presence in cold traps	LOLA PDS Data Node: https://imbrium.mit.edu/, [60]
WAC South Pole Summer Mosaic	100 m/pixel	Basemap	https://wms.lroc.asu.edu/lroc/view_rdr_product/WAC_ROI_SOUTH_SUMMER_100M, [63]
NAC Controlled South Pole Average Mosaic	1 m/pixel	Providing geological context for landing sites and identifying small impact craters	https://wms.lroc.asu.edu/lroc/view_rdr/NAC_POLE_SOUTH_CM_AVG, [90]
ShadowCam images	2 m/pixel	Providing geological context for sampling sites	https://data.ser.asu.edu/lunaserv.html, [81] Sampling site for de Gerlache-BL: M014056172S_map_stretched.tif Sampling site for de Gerlache-TL: M016355535S_map_stretched.tif; Sampling site for de Gerlache-TR: M016341390S_map_stretched.tif

			Sampling site for #12-TR: M014997797S_map_stretched.tif Sampling site for Faustini-BR: M017642527S_map_stretched.tif Sampling site for Shackleton-L: M014481615S_map_stretched.tif
LRO Mini-RF radar images (level1-CDR)	30 m/pixel	Identify rocky areas within landing and sampling sites	https://ode.rsl.wustl.edu/moon/productsearch, [82]

Table S2 Continued.

Table S2. List of the 61 potentially water-ice-bearing cold traps within a 300×300 km² square region, encompassing the circumpolar area south of 85°S, for the CE-7 mission.

CID[a]	Lon.[b] (°)	Lat.[b] (°)	Water ice detections[c]	LEND CSETN rate (cps)[d]
1	43.65	-88.02	166	4.849
2	-3.28	-87.47	94	4.879
3	83.35	-87.14	43	4.856
4	-143.11	-88.25	128	4.889
5	-47.31	-84.48	13	4.857
6	21.72	-86.78	30	4.900
7	113.49	-88.07	7	4.920
8	-91.77	-88.35	13	4.883
9	-177.71	-85.00	20	4.928
10	60.17	-84.56	17	4.908
11	128.04	-89.65	34	4.905
12	167.10	-88.71	39	4.888
13	-52.35	-85.44	1	4.881
14	31.55	-86.39	3	4.877
15	-47.41	-87.60	8	4.903
17	-44.21	-88.97	21	4.889
18	-21.98	-89.05	12	4.873
20	48.71	-85.39	7	4.917
21	118.91	-87.46	1	4.914
22	146.89	-88.35	6	4.905
23	18.21	-89.00	4	4.877
24	-31.08	-87.36	19	4.902

Table S2 Continued.

CID[a]	Lon.[b] (°)	Lat.[b] (°)	Water ice detections[c]	LEND CSETN rate (cps)[d]
25	-176.67	-88.45	5	4.899
26	-36.39	-84.60	2	4.886
27	-69.18	-84.95	4	4.915
29	123.91	-84.36	5	4.911
30	-14.53	-88.71	4	4.870
31	56.02	-84.36	10	4.941
33	-152.29	-84.44	4	4.950
34	-14.17	-86.06	1	4.889
35	-41.78	-85.39	1	4.894
36	47.86	-86.47	6	4.898
37	-122.32	-86.56	2	4.937
38	-93.04	-85.20	1	4.951
41	-74.87	-86.31	1	4.928
42	60.94	-86.79	3	4.883
43	-34.78	-87.82	3	4.900
46	-47.65	-87.26	1	4.909
47	-28.12	-88.54	8	4.869
49	-85.68	-89.50	9	4.926
50	150.54	-88.92	2	4.898
52	40.71	-87.15	1	4.877
53	47.89	-86.92	1	4.894
55	-97.58	-87.65	1	4.889
57	-150.43	-85.57	3	4.942
59	-113.45	-86.43	2	4.910

Table S2 Continued.

CID[a]	Lon.[b] (°)	Lat.[b] (°)	Water ice detections[c]	LEND CSETN rate (cps)[d]
61	-55.44	-85.08	1	4.891
63	-153.91	-85.28	4	4.958
65	-148.10	-85.68	3	4.930
72	-125.03	-86.27	1	4.946
73	-153.98	-84.83	2	4.959
76	68.19	-86.62	1	4.892
80	53.55	-86.79	2	4.896
81	-44.87	-88.68	2	4.884
86	-27.02	-87.57	4	4.903
88	-15.41	-85.83	1	4.888
93	19.39	-89.32	1	4.873
102	32.54	-86.97	2	4.890
104	129.18	-88.97	1	4.933
105	107.04	-85.69	1	4.948
121	33.85	-85.23	1	4.888

Note: [a]The cold trap ID corresponds to its rank in size among the 133 cold traps ($\geqslant$5 km^2) within a 300$\times$300 km^2 region centered on the lunar south pole. The 11 selected cold traps with a high potential for containing water ice are highlighted (1: Shoemaker, 2: Haworth, 3: Faustini, 4: Sverdrup, 5: Cabeus, 8: de Gerlache, 11: Shackleton). [b]The center location of the cold trap. [c]The count of water ice detections by a combination of M3, LOLA, and LAMP (see main text for details). [d]The LEND CSETN epithermal neutron count rate (count per second) collected between September 2009 and September 2016.

Table S3 Continued.

Table S3. Summary of characteristics of the landing regions, ranked based on a score calculated as the sum of the normalized landing site count and normalized average illumination.

Landing region name[a]	**Lon.**[b] **(°)**	**Lat.**[b] **(°)**	**Count**[c] **≤ 15 km**	**Slope 20 m baseline (°)**			**Illumination 60 m (%)**			**Representative Flight routes**[d]			**Score**[e]
				Avg.	**Med.**	Q_{95}	**Avg.**	**Med.**	Q_{95}	d **(km)**	h_{diff} **(km)**	$\theta_{descent}$ **(°)**	
de Gerlache-BL	-96.47	-87.94	52	7.6	7.1	14.5	39.0	41.1	49.0	8.3	2.3	12.1	1.54
#24-T	-26.95	-86.94	57	7.5	6.9	14.4	37.1	37.7	45.0	10.1	1.7	10.3	1.48
Faustini-BR	94.24	-86.72	55	7.4	6.7	15.4	37.2	39.9	48.6	11.2	2.4	14.4	1.45
de Gerlache-B	-110.50	-88.22	49	7.4	6.9	14.1	35.4	37.0	45.5	To de Gerlache			1.20
										6.1	1.4	11.7	
										To Sverdrup			
										13.9	2.3	3.3	
de Gerlache-TR	-68.46	-88.55	9	9.8	9.4	18.3	43.6	43.3	58.9	To de Gerlache			1.11
										9.2	2.5	9.1	
										To #17			
										13.0	2.9	12.7	
#12-TR	139.69	-88.79	22	8.0	7.8	13.5	39.5	40.9	48.8	8.5	1.6	10.9	1.03
Shackleton-L	-150.92	-89.84	5	15.2	13.3	30.9	43.3	42.3	65.5	8.0	4.3	10.0	1.01

Table S3 Continued.

Landing region name[a]	**Lon.**[b] **(°)**	**Lat.**[b] **(°)**	**Count**[c] **≤ 15 km**	**Slope 20 m baseline (°)**			**Illumination 60 m (%)**			**Representative Flight routes**[d]			**Score**[e]
				Avg.	**Med.**	Q_{95}	**Avg.**	**Med.**	Q_{95}	d **(km)**	h_{diff} **(km)**	$\theta_{descent}$ **(°)**	
de Gerlache-TL	-73.51	-88.13	20	7.8	7.1	15.9	39.6	41.8	50.5	4.4	1.2	14.3	1.00
Sverdrup-BR	-163.49	-87.89	8	10.1	9.5	20.1	41.9	44.0	56.9	8.0	2.0	9.2	0.96
Faustini-R	83.20	-86.41	16	7.0	6.6	13.2	36.8	39.2	50.2	13.6	3.5	10.2	0.70
Shackleton-TL	56.88	-89.78	6	11.1	10.1	23.6	39.1	39.2	54.9	7.0	3.7	20.0	0.70
de Gerlache-R	-95.49	-89.00	9	8.9	8.4	16.6	38.2	39.9	54.4	8.9	1.3	9.7	0.68
Cabeus-BL	-56.57	-84.31	20	7.0	6.7	13.3	35.6	36.9	38.5	10.0	1.6	10.7	0.67
Cabeus-TL	-48.20	-83.78	19	7.9	7.4	15.7	35.6	38.6	43.3	5.3	1.1	11.1	0.66
Faustini-B	99.60	-87.31	23	6.2	5.1	15.2	34.3	35.1	48.9	11.4	3.1	12.9	0.62
Faustini-BL	93.33	-87.78	17	7.1	6.5	14.3	35.0	36.8	51.0	12.1	2.9	11.7	0.58
Sverdrup-L	-130.76	-87.80	8	7.6	6.6	17.5	35.8	38.0	48.5	9.7	3.6	10.7	0.47
de Gerlache-BR	-108.87	-88.70	11	7.7	7.3	14.6	34.6	35.4	47.1	To de Gerlache			0.43
										4.4	0.8	12.2	
										To Sverdrup			
										13.2	2.2	11.1	
Cabeus-L	-54.40	-84.17	12	6.9	6.5	12.7	34.2	36.1	39.4	4.8	1.1	15.1	0.41

Table S3 Continued.

Landing region name[a]	Lon.[b] (°)	Lat.[b] (°)	Count[c] ≤ 15 km	Slope 20 m baseline (°)			Illumination 60 m (%)			Representative Flight routes[d]			Score[e]
				Avg.	Med.	Q_{95}	Avg.	Med.	Q_{95}	d (km)	h_{diff} (km)	$\theta_{descent}$ (°)	
#17-BL	-63.48	-88.72	4	8.2	7.9	14.3	35.5	36.9	44.6	8.9	2.2	12.7	0.37
Shackleton-R	106.18	-89.37	3	12.7	11.1	28.1	34.1	37.4	53.0	7.2	3.9	17.6	0.24
Shackleton-BR	130.96	-89.23	11	7.2	6.1	17.9	32.1	34.3	44.8	7.4	3.8	20.5	0.23
#12-BR	163.64	-88.33	14	6.8	6.1	14.1	31.4	34.0	45.1	10.6	1.5	7.7	0.23
Shackleton-BL	175.17	-89.52	5	12.1	10.8	25.2	33.3	34.7	54.1	7.5	3.9	21.4	0.21
#24-L	-37.05	-87.15	5	8.3	7.3	17.9	33.1	35.3	47.7	9.4	1.3	5.2	0.20
Faustini-L	76.96	-87.92	8	6.1	5.6	13.0	32.3	32.6	42.3	11.8	3.0	10.6	0.19
Shackleton-B	150.23	-89.36	5	10.4	9.4	23.3	33.0	37.9	47.5	6.8	3.6	21.1	0.19
Shackleton-TR	84.28	-89.52	3	10.2	8.9	22.1	32.9	37.6	46.9	7.3	4.2	25.3	0.14
#17-L	-53.45	-88.54	4	7.8	7.5	14.9	32.4	35.2	44.0	10.0	1.6	8.0	0.12
#12-T	161.19	-89.22	5	5.8	5.3	11.4	31.1	34.0	40.9	11.3	1.9	9.2	0.04

Note: [a]The name of each landing region combines the name of the cold trap it surrounds with its azimuthal direction relative to that cold trap. [b]The center location of the landing region. [c]The number of landing sites near cold traps (within a 15 km range) in the specified landing region. [d]The median values of key characteristics of feasible flight routes from each landing region to its accessible cold traps, including horizontal distance d, elevation difference between the landing and sampling regions $h_{diff} = h_{terrain}(0) - h_{terrain}(d)$, and the descent angle $\theta_{descent}$ over a 500 m baseline. [e]The landing region score is a combination of size and illumination; see main text for details.

Table S4. Statistics of the high-resolution illumination characteristics, fraction of cratered terrain, and fraction of rocky terrain for the selected landing regions. The DEMs used to simulate the illumination conditions have a resolution of 10 m/pixel for #24-T and Faustini-BR, and 5 m/pixel for the other regions. The average illumination represents the mean visible fraction of the solar disk from October 1, 2026, to October 1, 2034. LCIP and LCSP denote the longest continuous illuminated and shadowed periods, respectively, during the time frame from October 1, 2026, to October 1, 2027. Q_{95} represents the 95th percentile. LCIP and LCSP statistics for each landing region are calculated using pixels with an illumination of ⩾35% within the region.

Landing region	High-resolution illumination (%)			Fraction of area with illumination ≥ 35% (%)	LCIP (days)			LCSP (days)			Fraction of cratered terrain (%)	Expected Avg. illumination (%)	Fraction of rocky terrain (%)
	Avg.	Med.	Q_{95}		Avg.	Med.	Q_{95}	Avg.	Med.	Q_{95}			
de Gerlache-BL	34.9	37.4	45.6	62.4	15.2	15.2	16.9	19.1	18.8	21.9	11.3	32.0	4.7
#24-T	30.7	33.3	40.9	37.4	13.9	13.5	16.8	20.0	19.8	21.7	N/A	N/A	N/A
Faustini-BR	32.9	36.3	45.7	55.3	14.6	14.5	17.1	19.4	19.2	21.5	11.5	30.4	4.3
de Gerlache-B	30.8	33.4	41.0	39.2	14.9	14.8	17.0	20.0	20.2	21.8	N/A	N/A	N/A
de Gerlache-TR	36.0	38.1	47.3	64.8	15.6	15.1	18.7	19.4	18.8	22.1	16.2	31.0	0.3
#12-TR	36.2	38.1	45.8	64.4	15.0	15.0	16.6	18.5	18.3	20.6	13.5	31.6	0.9
Shackleton-L	35.2	36.4	42.6	64.3	14.9	14.6	17.5	18.4	18.0	21.2	16.4	29.1	2.1
de Gerlache-TL	34.9	37.4	46.0	59.4	15.2	15.1	17.8	19.6	19.0	22.6	12.6	30.9	8.1